

Geometry-Based Data Generation

Ofir Lindenbaum^{1,2*} Jay S. Stanley III^{1,3} Guy Wolf^{2†}
Smita Krishnaswamy^{1,4†}

¹Department of Genetics; ²Applied Mathematics Program;

³Computational Biology & Bioinformatics Program;

⁴Department of Computer Science;

Yale University, New Haven, CT, USA

*Corresponding author. E-mail: ofir.lindenbaum@yale.edu

Address: 333 Cedar St, New Haven, CT 06510, USA

† These authors contributed equally.

May 18, 2022

Abstract

Many generative models attempt to replicate the density of their input data. However, this approach is often undesirable, since data density is highly affected by sampling biases, noise, and artifacts. We propose a method called SUGAR (Synthesis Using Geometrically Aligned Random-walks) that uses a diffusion process to learn a manifold geometry from the data. Then, it generates new points evenly along the manifold by pulling randomly generated points into its intrinsic structure using a diffusion kernel. SUGAR equalizes the density along the manifold by selectively generating points in sparse areas of the manifold. We demonstrate how the approach corrects sampling biases and artifacts, while also revealing intrinsic patterns (e.g. progression) and relations in the data. The method is applicable for correcting missing data, finding hypothetical data points, and learning relationships between data features.

1 Introduction

Many types of data analysis suffer from what is known as “imbalanced data” or biased sampling of data from a system. Statistical methods such as mutual information are highly weighted by density and thus can mis-quantify the strength of dependencies with data whose density is concentrated in a particular region of the relationship. For example, in immunology, if the activity of a t-cell stimulatory molecule and its respondent inflammatory cytokines is mostly observed in an off state, statistical measures will be biased towards negligible dependency, despite the true positive relationship between t-cell stimulation and inflammation. In principle component analysis, major components (eigenvectors of the covariance matrix) can

span data points of a particular type if they are oversampled. For instance, if healthy individuals form 99 percent of a sample then PC components may span variation in healthy individuals rather than the gradient between healthy and sick patients. In supervised learning, some classifiers tend to bias towards the classes with highest density [He & Garcia \(2009\)](#); [López et al. \(2013\)](#); [Hensman & Masko \(2015\)](#). The rare samples, on the other hand, are often the interesting ones [Weiss \(2004\)](#). Some examples for such cases include learning pronunciations of words [Van Den Bosch et al. \(1997\)](#), finding fraud credit card transactions [Chan & Stolfo \(1998\)](#) and identifying earthquakes from seismic recordings [Lindenbaum et al. \(2017a\)](#).

The general problem in these examples is that density is conflated with importance of samples when in fact rare samples are often of great interest [Weiss \(2004\)](#). While oversampling can often be corrected, under-sampling is harder to emend. Density may originate from data existence as much as sample bias. Most other generative models attempt to learn and replicate the density of the data, which is not only intractable in high dimensions but also exacerbates this problem. Examples for such methods include Gaussian Mixture Models (GMM) [Rasmussen \(2000\)](#), variational Bayesian methods [Bernardo et al. \(2003\)](#), kernel density estimates [Scott \(2008\)](#).

We assume that the sampled data lie on low-dimensional manifolds. Based on this, we propose a new type of generation method termed SUGAR (Synthesis Using Geometrically Aligned Random-walks) that learns the underlying manifold geometry of the data. Under-sampled regions within the manifold geometry can be regenerated using this structure. We learn the manifold by using a diffusion operator or a kernel that requires only the computation of pairwise affinities between data points. Then, we generate new points randomly around existing points. Finally, we apply a weighted transition kernel to pull the new points towards the structure of the manifold, especially in sparse areas.

There are several advantages of this approach over traditional generative models which learn a probability density estimate of the data. These include 1) the ability to compensate for sparsity and heavily biased sampling in many data types of interest, especially biomedical data, 2) increased representational efficiency: multivariate probability distributions are very difficult, if not impossible, to represent accurately in high dimensions. Usually, vast simplifications such as parametric forms or restriction to marginals have to be used in order to make distribution-based generative models tractable. We apply our method for generating data based on unevenly sampled artificial and biological data-sets. Results show that the data generated by our methods is smooth, less noisy, fills in holes in the manifold, and more evenly sampled compared to the original points.

2 Problem Formulation

Let \mathcal{M} be a d dimensional manifold that lies in a higher dimensional space \mathbb{R}^D , with $d < D$, and let $\mathbf{X} \subseteq \mathcal{M}$ be a dataset of $N = |\mathbf{X}|$ data points, denoted $\mathbf{x}_1, \dots, \mathbf{x}_N$, sampled from the manifold. In this paper, we propose an approach that uses the samples in \mathbf{X} in order to capture the manifold geometry and generate new data points from the manifold. In particular, we focus on the case where the points in \mathbf{X} are unevenly sampled from \mathcal{M} , and aim to generate a set of M new data points $\mathbf{Y} = \{\mathbf{y}_1, \dots, \mathbf{y}_M\} \subseteq \mathbb{R}^D$ such that 1. the new points \mathbf{Y} approximately lie on the

manifold \mathcal{M} , and 2. the distribution of points in the combined dataset $\mathbf{Z} \triangleq \mathbf{X} \cup \mathbf{Y}$ is uniform. Our proposed approach is based on using intrinsic diffusion process over the manifold to define a diffusion geometry (see Section 3) that robustly captures the manifold geometry even from \mathbf{X} . Then, we use this diffusion process to generate new data points that follow the manifold geometry while adjusting their intrinsic distribution, as explained in Section 4.

3 Background

In this section we briefly describe the mathematical background required for this study.

3.1 Diffusion Geometry

A popular approach to robustly capture an intrinsic manifold geometry from sampled data is based on diffusion geometry. This approach exploits a Markovian random walk to capture nonlinear relations in the data. The non-linear dimensionality reduction algorithm Diffusion Maps (DM) uses this technique [Coifman & Lafon \(2006\)](#). The diffusion geometry utilized in DM is based on first defining a kernel that captures local neighborhoods in the data, such as the Gaussian kernel

$$\mathcal{K}(\mathbf{x}_i, \mathbf{x}_j) \triangleq K_{i,j} = \exp\left(-\frac{\|\mathbf{x}_i - \mathbf{x}_j\|^2}{2\sigma^2}\right), i, j = 1, \dots, N \quad (1)$$

where σ is a user-configurable parameter that controls the neighborhood sizes. Then, a diffusion operator is defined as the row-stochastic matrix $P_{i,j} = \mathcal{P}(\mathbf{x}_i, \mathbf{x}_j) = [\mathbf{D}^{-1}\mathbf{K}]_{i,j}$, $i, j = 1, \dots, N$, where \mathbf{D} is a diagonal matrix with values corresponding to the degree of the kernel $D_{i,i} = \hat{d}(i)$. The degree of the kernel is defined as

$$\hat{d}(i) = \sum_j \exp\left(-\frac{\|\mathbf{x}_i - \mathbf{x}_j\|^2}{2\sigma^2}\right), i = 1, \dots, N. \quad (2)$$

The degree value $\hat{d}(i)$ at each point indicates the amount of connectivity the point has to its neighbors. The matrix \mathbf{P} defines an imposed diffusion process, whose transition probabilities are given by the matrix elements. As was shown in [Coifman & Lafon \(2006\)](#), the matrix \mathbf{P} efficiently captures the diffusion geometry of a manifold \mathcal{M} .

The DM framework also enables reducing the dimension of complex datasets while preserving diffusion geometry. The embedding provided by DM is given by the eigendecomposition of the diffusion operator as $\Psi(\mathbf{x}_i) = [\lambda_1\psi_1(i), \lambda_2\psi_2(i), \dots, \lambda_d\psi_d(i)]^T$ where $1 = \lambda_0 \geq \lambda_1 \geq \dots \geq \lambda_d$ are the eigenvalues of \mathbf{P} , $\psi_0, \psi_1, \dots, \psi_d$ are the corresponding eigenvectors, and d is the dimensionality of the embedded space, typically determined by the numerical rank of \mathbf{P} . Note that the trivial all ones eigenvector ψ_0 has been excluded from the DM representation. In this paper, we do not directly use the diffusion embedding of DM, but rather a variant of the operator \mathbf{P} that captures diffusion geometry. In section 4, we explain how this operator allows us to ensure the data we generate follows diffusion geometry and the manifold structure it represents.

3.2 Measure Based Gaussian Correlation

In [Bermanis et al. \(2016\)](#), a Measure-based Gaussian Correlation (MGC) kernel is suggested as an alternative to the Gaussian kernel (Eq. 1) for constructing diffusion geometry. The MGC diffusion operator is formulated by incorporating local affinities with a measure μ . The measure could be provided in advance or approximated based on the data samples. The MGC kernel with a measure $\mu(\mathbf{r})$ is defined using the following equation

$$\hat{\mathcal{K}}(\mathbf{x}_i, \mathbf{x}_j) = \sum_{\mathbf{r} \in \mathcal{X}} \mathcal{K}(\mathbf{x}_i, \mathbf{r}) \mathcal{K}(\mathbf{r}, \mathbf{x}_j) \mu(\mathbf{r}), i, j = 1, \dots, M, \quad (3)$$

where the kernel \mathcal{K} is some decaying symmetric function. In this study we use the radial basis function kernel (defined in Eq. 1).

3.3 Kernel Bandwidth Selection

The choice of kernel bandwidth σ (Eq. 1) is crucial for the performance of kernel methods. For small values of σ the kernel \mathcal{K} (Eq. 1) converges to the identity matrix; inversely, large values of σ yield the all ones matrix. Many methods have been proposed for tuning σ . A range of values is suggested in [Singer et al. \(2009\)](#) based on an analysis of the sum of \mathcal{K} . In [Lindenbaum et al. \(2017b\)](#) a method is presented dedicated for classification or manifold learning. We describe two methods for setting the bandwidth, a global scale suggested in [Keller et al. \(2010\)](#) and an adaptive local scale based on [Zelnik-Manor & Perona \(2005\)](#). As a global scale, we use the max-min bandwidth [Keller et al. \(2010\)](#) as it is simple and effective. The max-min bandwidth is defined by $\sigma_{\text{MaxMin}}^2 = \mathcal{C} \cdot \max_j [\min_{i, i \neq j} (\|\mathbf{x}_i - \mathbf{x}_j\|^2)]$, where $\mathcal{C} \in [2, 3]$. This approach attempts to force that each point is connected to at least one other point. This method is simple, but highly sensitive to outliers. An adaptive bandwidth is proposed in [Zelnik-Manor & Perona \(2005\)](#). At each point, the scale is chosen as the L_1 distance from the r th nearest neighbor of the point \mathbf{x}_i . Explicitly, the calculation for each point is $\sigma_i = \|\mathbf{x}_i - \mathbf{x}_r\|$, where \mathbf{x}_r is the r th nearest neighbor of the point \mathbf{x}_i . The value of the kernel for points \mathbf{x}_i and \mathbf{x}_j is

$$\mathcal{K}(\mathbf{x}_i, \mathbf{x}_j) \triangleq K_{i,j} = \exp\left(-\frac{\|\mathbf{x}_i - \mathbf{x}_j\|^2}{\sigma_i \sigma_j}\right). \quad (4)$$

This adaptive bandwidth guarantees that at least half of the points are connected to r neighbors. The exact choice should be tailored to the dataset, if the density is highly biased the adaptive scale is preferable.

4 Data Generation

In this section, we detail the proposed method named SUGAR: Synthesis Using Geometrically Aligned Random-walks. SUGAR uses the MGC diffusion operator (Eq. 3) to generate synthetic data uniformly along the manifold \mathcal{M} . This is done by creating additional points in sparse regions and pulling them towards the manifold using an imposed Random-walk.

4.1 SUGAR: Synthesis Using Geometrically Aligned Random-walks

SUGAR initializes by synthesizing new points around sparse areas of the manifold to create a new set of points \mathbf{Y}_0 . We draw each new point $\mathbf{y}_i \in \mathbf{Y}_0, i = 1, \dots, M$ from a Gaussian distribution designed to maintain the local structure. Each Gaussian $\mathcal{N}(\mathbf{x}_i, \Sigma_i)$ is centered around an existing point \mathbf{x}_i and has a local covariance structure Σ_i . The local covariance Σ_i is the sample covariance based on k nearest neighbors surrounding \mathbf{x}_i . Thus, we elaborate the local structure of the manifold to generate points in the meaningful directions. Then, we construct an operator $\hat{\mathbf{P}}$ (Eq. 6) which imposes a weighted random walk model between new points \mathbf{Y}_0 and original points \mathbf{X} . This is done using the affinities in the sampled set \mathbf{X} , and the generated set \mathbf{Y}_0 . To pull the new points toward the sparse regions of the manifold \mathcal{M} we use a sparsity measure $\mu(\mathbf{x}_i) \triangleq \hat{s}(i), i = 1, \dots, N$. The sparsity based MGC kernel is defined as

$$\hat{\mathcal{K}}(\mathbf{y}_i, \mathbf{y}_j) = \sum_{\ell} \mathcal{K}(\mathbf{y}_i, \mathbf{x}_{\ell}) \mathcal{K}(\mathbf{x}_{\ell}, \mathbf{y}_j) \hat{s}(\ell), i, j = 1, \dots, M. \quad (5)$$

The kernel $\hat{\mathcal{K}}$ is normalized using a diagonal matrix $\hat{\mathbf{D}}$, such that $\hat{D}_{i,i} = \sum_j \hat{K}_{i,j}$. Finally, the sparsity based diffusion operator is computed by

$$\hat{\mathbf{P}} = \hat{\mathbf{D}}^{-1} \hat{\mathcal{K}}. \quad (6)$$

By applying the operator $\hat{\mathbf{P}}^t$ to a set of new points \mathbf{Y}_0 each point is locally averaged based on its neighbors in $\mathbf{X} \subset \mathcal{M}$. The time parameter t controls the number of diffusion steps taking place. Applying the operator at time instant t effectively performs a low pass on the noisy generated data \mathbf{Y}_0 . The number of steps required can be set manually or using the Von Neumann Entropy as was suggested in Moon et al. (2017). In the final step, data is rescaled to fit the range of original values of \mathbf{X} .

We suggest to use the degree $\hat{d}(i)$ to define sparsity of each point, as degree measures the connectivity of each point to its neighborhood. The proposed sparsity is defined by

$$\hat{s}(i) \triangleq \frac{1}{\hat{d}(i)}, i = 1, \dots, N. \quad (7)$$

Clearly $\hat{s}(i) \geq 0, i = 1, \dots, N$, as the degree $\hat{d}(i)$ at each point is non-negative (see Eq. 2). Here, we proposed a simple sparsity measure, however one may consider a more complex choice given prior knowledge about sampling distribution bias. A full description of the approach is given in Algorithm 1.

4.2 Manifold Density Equalization

The amount of points $\hat{\ell}(i)$ (step 4 in Algorithm 1) generated around each \mathbf{x}_i affects the distribution of points in \mathbf{Y}_1 . Here we present a method for approximating the number of points $\hat{\ell}(i)$ required for equalizing the distribution of points. By equalizing we mean that the density of generated points over \mathcal{M} is uniform. Given a biased data set our goal is to generate more points at sparse regions to balance the non-uniform density of \mathbf{X} . To do this we have proposed to draw $\hat{\ell}(i)$ points around each point $\mathbf{x}_i, i = 1, \dots, N$ from $\mathcal{N}(\mathbf{x}_i, \Sigma_i)$ (as described in Algorithm 1). The following

Algorithm 1 SUGAR: Synthesis Using Geometrically Aligned Random-walks

Input: Dataset $\mathbf{X} = \{\mathbf{x}_1, \mathbf{x}_2, \dots, \mathbf{x}_N\}, \mathbf{x}_i \in \mathbb{R}^D$.

Output: Generated set of points $\mathbf{Y} = \{\mathbf{y}_1, \mathbf{y}_2, \dots, \mathbf{y}_M\}, \mathbf{y}_i \in \mathbb{R}^D$.

- 1: Compute the diffusion geometry operators \mathbf{K}, \mathbf{P} (Eqs. 1 and 3.1) and the degrees $\hat{d}(i), i = 1, \dots, N$ (Eq. 2).
- 2: Define a sparsity measure $\hat{s}(i), i = 1, \dots, N$.
- 3: Estimate a local covariance $\Sigma_i, i = 1, \dots, N$ using k nearest neighbors around \mathbf{x}_i .
- 4: For each point $i = 1, \dots, N$ draw $\hat{\ell}(i)$ vectors from a Gaussian distribution $\mathcal{N}(\mathbf{x}_i, \Sigma_i)$.
- 5: Compute the sparsity based diffusion operator $\hat{\mathbf{P}}$ defined in Eq. 6.
- 6: Apply the operator $\hat{\mathbf{P}}$ at time instant t to the new generated points $\hat{\mathbf{Y}}_0$. Such that the diffused points are defined as $\mathbf{Y}_t = \hat{\mathbf{P}}^t \cdot \mathbf{Y}_0$
- 7: Rescale \mathbf{Y}_t to fit the range of the original data based on the following equation:

$$\mathbf{Y} = \mathbf{Y}_t \cdot \frac{\text{percentile}(\mathbf{X}, .99)}{\max \mathbf{Y}_t} \quad (8)$$

proposition provides the “correct” number of points $\hat{\ell}(i), i = 1, \dots, N$ required to balance the density over the manifold by equalizing the degrees $\hat{d}(i)$ (Eq. 2).

Proposition 4.1. *For each point $\mathbf{x}_i \in \mathcal{M} \setminus \partial\mathcal{M}$ the expectation value of the degree $\hat{d}(i)$ is constant if the number of points generated is given by*

$$\hat{\ell}(i) = \lfloor \det(\Sigma_i^{-1} + \frac{\mathbf{I}}{2\sigma^2})^{0.5} \det(\Sigma_i)^{0.5} [\max(\hat{d}(\cdot)) - \hat{d}(i)] \rfloor, \quad (9)$$

where $\hat{d}(i)$ is the degree value at point \mathbf{x}_i , σ^2 is the bandwidth of the kernel \mathbf{K} (Eq. 1) and Σ_i is the covariance of the Gaussian designed for generating new points (as described in Algorithm 1).

Proof. Given $\mathbf{x}_i \in \mathbb{R}^D, i = 1, \dots, N$, the degree at point \mathbf{x}_i is defined in Eq. 2. SUGAR (Algorithm 1) generates $\hat{\ell}(i)$ points around \mathbf{x}_i from a Gaussian distribution $\mathcal{N}(\mathbf{x}_i, \Sigma)$. After generating $\hat{\ell}(i)$ points, the degree at point \mathbf{x}_i is defined as

$$\hat{d}(i) = \sum_{j=1}^N e^{-\frac{\|\mathbf{x}_i - \mathbf{x}_j\|^2}{2\sigma^2}} + \sum_{\ell=1}^{\hat{\ell}(i)} e^{-\frac{\|\mathbf{x}_i - \mathbf{y}_\ell^i\|^2}{2\sigma^2}}. \quad (10)$$

In order to equalize the distribution, we require that the expectation of the degree be independent of x_i , thus, we set $\mathbb{E}[\hat{d}(i)] = C, i = 1, \dots, N$, where C is a constant that will be addressed later in the proof. Further, we notice that the first term in the right hand side of Eq. 10 can be substituted by $\hat{d}(i)$, while the second term is a sum of $\hat{\ell}(i)$ random variables. For simplicity, we assume at this point that the points generated around \mathbf{x}_i have negligible effect on the $\hat{d}(j)$ at point $j \neq i$. We note that this assumption should hold with proper choices of σ and $\Sigma_i, i = 1, \dots, N$. By substituting the constant C , the term $\hat{d}(i)$, and using the independence assumption, the expectation of Eq. 11 can be written as

$$C - \hat{d}(i) = \mathbb{E} \left[\sum_{\ell=1}^{\hat{\ell}(i)} e^{-\frac{\|\mathbf{x}_i - \mathbf{y}_\ell^i\|^2}{2\sigma^2}} \right]. \quad (11)$$

Then, since the variables \mathbf{y}_i^i are i.i.d., then the right hand side of Eq. 11 becomes

$$\hat{\ell}(i) \mathbb{E} \left[e^{-\frac{\|\mathbf{x}_i - \mathbf{y}^i\|^2}{2\sigma^2}} \right] = \frac{\hat{\ell}(i)}{\det(2\pi\boldsymbol{\Sigma}_i)^{1/2}} \int_{\mathbb{R}^D} e^{-\frac{\|\mathbf{x}_i - \mathbf{y}^i\|^2}{2\sigma^2}} e^{-(\mathbf{x}_i - \mathbf{y}^i)^T \boldsymbol{\Sigma}_i^{-1} (\mathbf{x}_i - \mathbf{y}^i)} d\mathbf{y}^i,$$

and then using a change of variables $\tilde{\mathbf{y}} = \mathbf{y}^i - \mathbf{x}_i$, the integral simplifies to

$$\frac{\hat{\ell}(i)}{\det(2\pi\boldsymbol{\Sigma}_i)^{1/2}} \int_{\mathbb{R}^D} e^{-(\mathbf{x}_i - \mathbf{y}^i)^T (\boldsymbol{\Sigma}_i^{-1} + \frac{\mathbf{I}}{2\sigma^2}) (\mathbf{x}_i - \mathbf{y}^i)} d\mathbf{y}^i = \frac{\hat{\ell}(i)}{\det(\boldsymbol{\Sigma}_i^{-1} + \frac{\mathbf{I}}{2\sigma^2})^{0.5} \det(\boldsymbol{\Sigma}_i)^{0.5}},$$

where the final step is based on the integral of a Gaussian and a change of variables. Finally, we conclude that the estimator for the number of points $\hat{\ell}(i)$ is $\hat{\ell}(i) = \lfloor \det(\boldsymbol{\Sigma}_i^{-1} + \frac{\mathbf{I}}{2\sigma^2})^{0.5} \det(\boldsymbol{\Sigma}_i)^{0.5} [C - \hat{d}(i)] \rfloor$. By choosing $C = \max(\hat{d}(\cdot))$ we guarantee that $\hat{\ell}(i) \geq 0$ (which means that we are not removing points). In section 5.1 we demonstrate the proposed approach for density equalization. \square

5 Experimental Results

In this section we describe the experimental evaluation of SUGAR (Algorithm 1).

5.1 Density Equalization

In the following experiment we evaluate the proposed method for density equalization, as explained in Section 4.2) based on Proposition 4.1, which provides a method for choosing the number of generated points $\hat{\ell}(i)$ at each region on the manifold. We start by sampling a hundred points from a circle (see Fig. 2) such that the highest density is at the origin ($\theta = 0$) and the density decreases away from it. Figure 1(a) shows each point x_i colored by its degree $\hat{d}(i)$ (as defined in Eq. 2). Figure 2(b) shows new points generated based on $\hat{\ell}(i)$ around each original point.

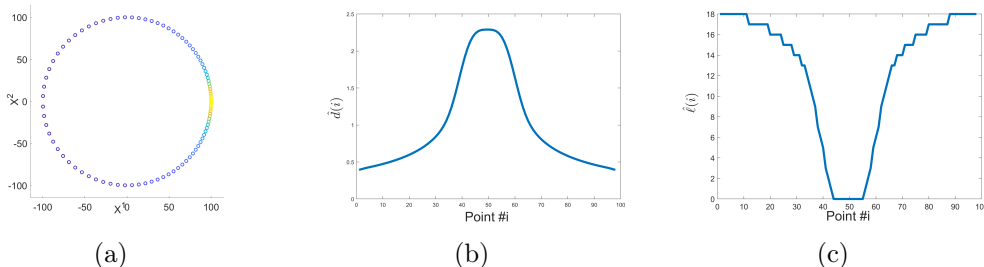


Figure 1: Density equalization demonstrated on a circle shaped manifold. (a) The original non-uniform samples of \mathbf{X} . (b) The degree value $\hat{d}(i)$ at each point $\mathbf{X}_i, i = 1, \dots, 100$. (c) The number of generated points $\hat{\ell}(i), i = 1, \dots, 100$.

We then apply SUGAR and estimate the CDF of \mathbf{X} and \mathbf{Z} based on a projection of the points to the first coordinate. We note that the resulting distribution shown

in blue is approximately a density of a standard uniform CDF as shown in red in Fig. 2(c). The variance of the degree $\hat{d}(\cdot)$ drops from 0.45 to 0.03, yet another indication of the improved density of points.

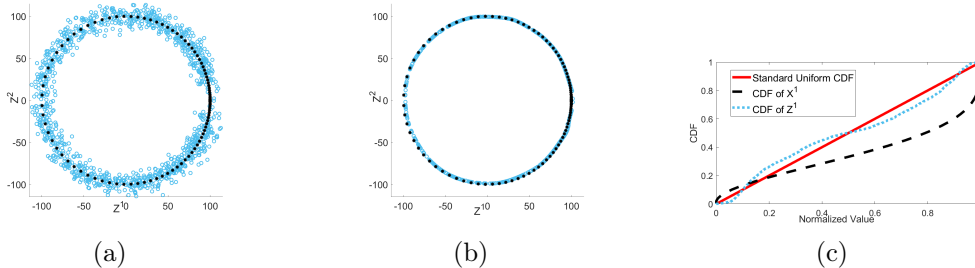


Figure 2: Density equalization demonstrated on a circle shaped manifold. (a) The original points \mathbf{X} (black asterisks) and set of new generated points \mathbf{Y}_0 (blue circles). (b) The final set of points \mathbf{Z} , original points \mathbf{X} (black asterisks) and set of new generated points \mathbf{Y}_t (blue circles). In this example only one diffusion time step is required (i.e. $t = 1$). (c) An estimation of the CDF before (black asterisks) and after (blue circles) applying the SUGAR compared to the CDF of a standard uniform distribution.

5.2 Artificial Manifolds

In the next experiment, we evaluate SUGAR on a Swiss roll, a popular manifold widely used for non-linear dimensionality reduction. We apply SUGAR to a non-uniformly generated Swiss roll. The Swiss roll \mathbf{X} is generated by applying the following construction steps:

- The random variables $\theta_i, h_i, i = 1, \dots, N$, are drawn from the distributions $P(\theta), P(h)$ respectively.
- A 3-dimensional Swiss roll is constructed based on the following function

$$\mathbf{X}_i = \begin{bmatrix} x_i^1 \\ x_i^2 \\ x_i^3 \end{bmatrix} = \begin{bmatrix} 6\theta_i \cos(\theta_i) \\ h_i \\ 6\theta_i \sin(\theta_i) \end{bmatrix}, i = 1, \dots, N. \quad (12)$$

In Fig. 3(a) we show a Swiss roll where $\theta_i, i = 1, \dots, N$ is drawn from a nonuniform distribution within the range $[\frac{3\pi}{2}, \frac{9\pi}{2}]$. Density of points decreases at higher values of θ_i . The values $h_i, i = 1, \dots, N$ are drawn from a uniform distribution within the range $[0, 20]$ and we use $N = 600$ points.

The Swiss roll is 3-dimensional but governed by one angular parameter. Thus, it allows us to evaluate whether SUGAR generates points uniformly along the Swiss roll's angular parameter. In the following, we apply Alg. 1 to the Swiss roll presented in Fig. 3(a). In Fig. 3(b) we present the original data \mathbf{X} and the generated points \mathbf{Y}_0 . The points are generated based on steps 1-4 in Alg. 1. After applying the MGC diffusion operator the points are pulled toward the Swiss roll structure. The points after applying the MGC operator $\hat{\mathbf{P}}$ (Eq. 5) are presented in Fig. 3(c). In these figures the points are colored by their degree value $\hat{d}(i)$. In Fig. 3(d) we present

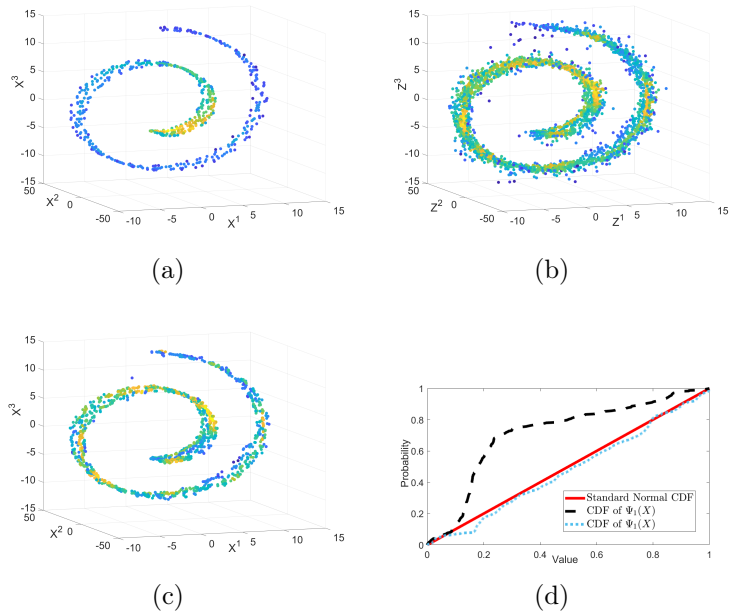


Figure 3: (a) A Swiss roll generated using Eq. 12. The variables h_i are drawn from uniform distribution within the interval $[0, 100]$, while θ_i are drawn from a nonuniform distribution. Points are colored by their degree value $\hat{d}(i)$. (b) The Swiss roll \mathbf{X} (black asterisk) and new generated points \mathbf{Y}_0 (blue circle). Points are generated based on step 4 in Alg. 1. (c) The points after applying the MGC operator $\hat{\mathbf{P}}^t$ (steps 6-7 Alg. 1). Only one diffusion time step is required (i.e. $t = 1$). (d) An estimate of the CDF based on the first embedding (DM) coordinate of $\mathbf{X} \cup \mathbf{Y}$.

the estimated CDF before and after applying SUGAR to \mathbf{X} . The resulted CDF resembles the CDF of a uniform distribution plotted in red. The variance of the degree $\hat{d}(i)$ drops from 0.19 to 0.09 when comparing \mathbf{X} and \mathbf{Z} .

5.3 MNIST Manifold

In the following experiment, we use an image from MNIST to generate an artificial low dimensional manifold in a high dimensional pixel space. We select an example of a handwritten '6' and rotate it in $N = 320$ different angles θ_i picked from a non uniform distribution within the range of $[0, 2\pi]$ to generate points $\mathbf{X} = \{\mathbf{x}_1, \mathbf{x}_2, \dots, \mathbf{x}_N\}$. Thus, by construction, the underlying latent parameter generating the data of \mathbf{X} is the angle θ . To learn the structure of the circular manifold that governs \mathbf{X} , we apply DM and present the two leading coordinates. This DM, colored by the degree value $\hat{d}(i)$, is presented in Fig. 5(a). We generate $\hat{\ell}(i)$ points around each $\mathbf{x}_i, i = 1, \dots, N$ based on the method presented in Algorithm 1 and Section 4.2. An example of a new point from \mathbf{Y}_0 is presented in Fig. 4(c). In the final step, we apply the operator $\hat{\mathbf{P}}$ to the set of new points \mathbf{Y}_0 . An example of a point from the set \mathbf{Y} is presented in Fig. 4(d), where it is evident that applying $\hat{\mathbf{P}}$ has cleaned the generated image in pixel space.

To further evaluate the performance of SUGAR, we examine the DM representation of \mathbf{Y}_0 and \mathbf{Y} . The results are presented in Figures 5(c) and 5(d) correspondingly. As depicted by Fig. 5(c), SUGAR has indeed maintained the structure

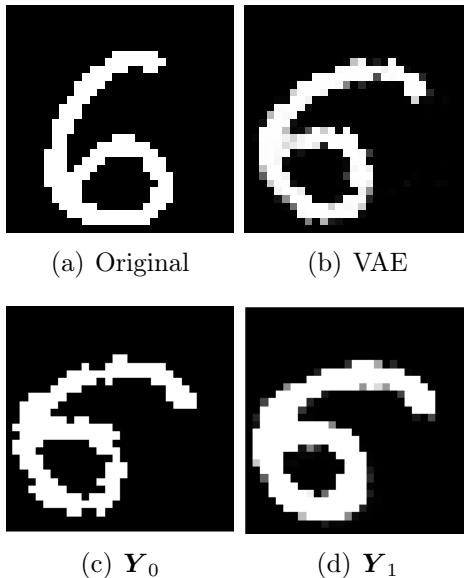


Figure 4: (a) The input image of a handwritten digit $\mathbf{x}_0 \in \mathbb{R}^{30 \times 30}$. (b) An example of an image generated using a Variational Auto Encoder (VAE). (c) An example of a synthesized image, drawn from a Gaussian distribution as described in step 4 of Alg. 1. (d) The same image as in (c) after applying the MGC diffusion operator $\hat{\mathbf{P}}$ (steps 6-7 of Alg. 1).

of the original manifold \mathcal{M} and generated points at the sparse regions of \mathbf{X} . We compare our result to Variational Auto Encoders (VAE) [Kingma & Welling \(2013\)](#), the training is performed on \mathbf{X} using two layers. An example of the networks output is presented in Fig. 4(b). A DM representation of the images generated from the VAE is presented in Fig. 5(b). The VAE does not fill in holes or sparse areas of the manifold but tends to generate points similar to the original points. By contrast SUGAR does fill in missing rotations of '6'.

5.4 Bunny Manifold

In the following experiment, we evaluate the performance of SUGAR on the “Stanford Bunny”. The “Stanford Bunny” is a set of points representing a 3-d surface of a bunny. We subsample the points on the surface such that the unevenly sampled set of points \mathbf{X} consists of 900 points. The data set \mathbf{X} colored by the degree estimate at each point is presented in Fig. 6(a). Then, we generate a set of new points \mathbf{Y}_0 based on steps 1-4 of Algorithm 1. The unified set of points $\mathbf{X} \cup \mathbf{Y}_0$ is presented in Fig. 6(b). In the final step, we apply the MGC operator \mathbf{P}^t , at $t = 1$, the final set of points $\mathbf{Z} = \mathbf{X} \cup \mathbf{Y}$ is presented in Fig. 6(c). The set \mathbf{Z} colored by the degree value $\hat{d}(i)$ is presented in Fig. 6(d).

In this experiment, the output of SUGAR has preserved the complex structure of the 3-d Bunny manifold. The variance of the degree $\hat{d}(i)$ in this example, drops from 0.24 to 0.019 when comparing \mathbf{X} and \mathbf{Z} .

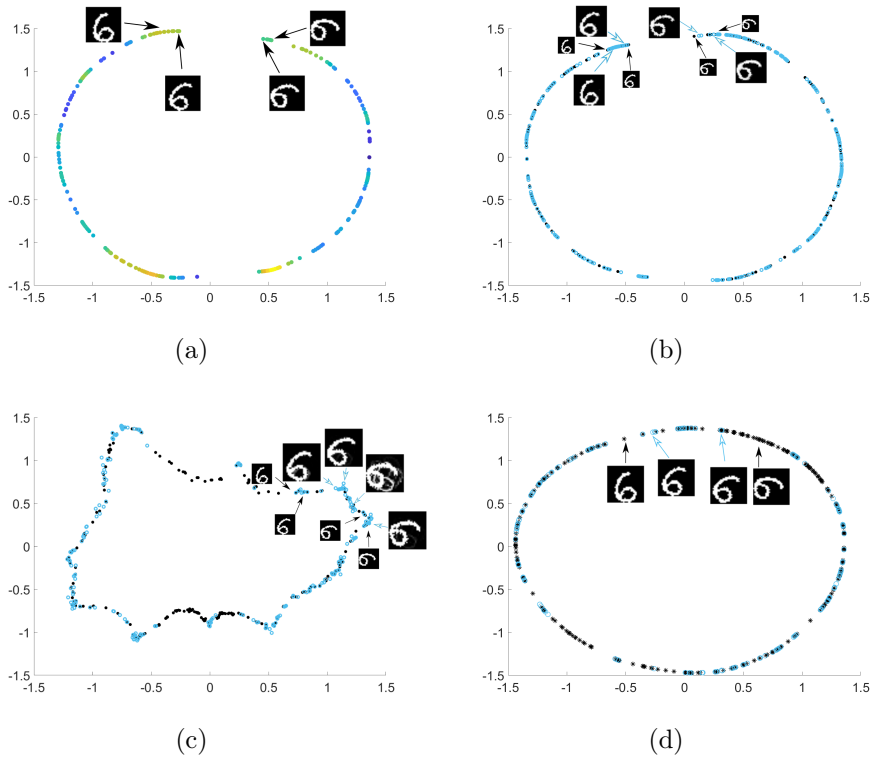


Figure 5: A 2-dimensional DM representation of: (a) \mathbf{X} , representing 320 rotated images of handwritten '6'. Points are colored by the degree value $d(i)$. (b) The output of the VAE, blue circles and the original points \mathbf{X} black asterisks. (c) The unity set $\mathbf{X} \cup \mathbf{Y}_0$, black asterisks- \mathbf{X} original points, blue circles- new points \mathbf{Y}_0 . (d) The final set $\mathbf{X} \cup \mathbf{Y}$, using $t = 1$. \mathbf{Y} is the set of generated points after applying the MGC diffusion operator $\hat{\mathbf{P}}$ (steps 6-7 of Alg. 1).

5.5 Biological Manifolds

In this section, we apply SUGAR to a biological dataset collected by [Velten et al. \(2017\)](#). [Velten et al. \(2017\)](#) present a model of cellular development in which a central reservoir of stem cells gives rise to unique, continuous trajectories, each leading to functionally distinct mature cells. This branching geometry thus lends itself to exploration using manifold learning.

This dataset presents four distinct challenges. First, each cell contains two measurement types, single cell RNA sequencing (scRNA-seq)

$\mathbf{X}_{\text{scrna}} = \{\tilde{\mathbf{x}}_1, \tilde{\mathbf{x}}_2, \dots, \tilde{\mathbf{x}}_{1029}\}, \tilde{\mathbf{x}}_i \in \mathbb{R}^{12553}$, and indexed fluorescence activated cell sorting (FACS), ($\mathbf{X}_{\text{facs}} = \{\hat{\mathbf{x}}_1, \hat{\mathbf{x}}_2, \dots, \hat{\mathbf{x}}_{1029}\}, \hat{\mathbf{x}}_i \in \mathbb{R}^8$). Ideally, these two data types must be integrated together for accurate analysis. Second, the [Velten et al. \(2017\)](#) dataset is small: only 1029 cells are measured in one individual, making the data generally sparse and hard to visualize. Third, many rare populations exist in the dataset. Fourth, branch discontinuities concentrate sparsity in the data along developmental branches, leading to large gaps in data space between immature cells and their mature counterparts.

[Velten et al. \(2017\)](#) visualize this data using a supervised technique in which data points are projected onto arms of a star-like shape using similarity scores to previously identified gene signatures [Velten et al. \(2017\)](#). We recapitulated this shape using the unsupervised dimensionality reduction technique PHATE to gener-

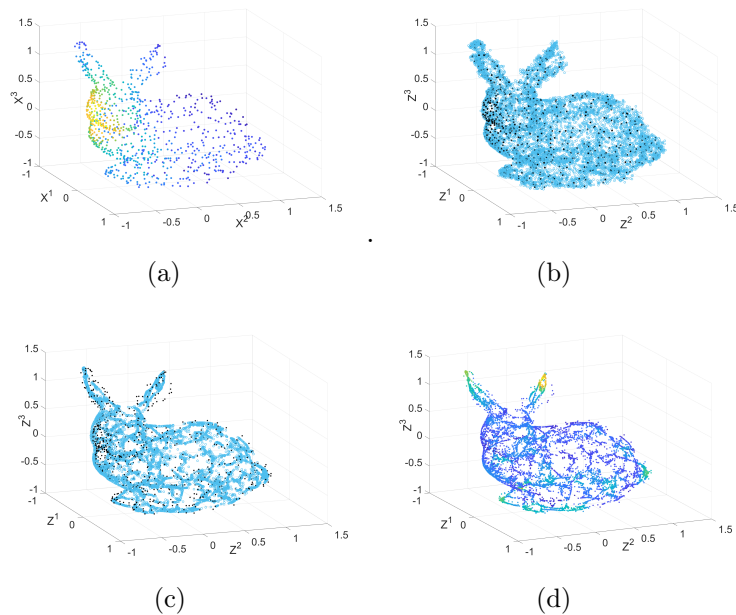


Figure 6: (a) A subset \mathbf{X} with 900 points from the Stanford Bunny. Points are colored by their degree value $\hat{d}(i)$. (b) The original and generated points $\mathbf{X} \cup \mathbf{Y}_0$, black asterisks- \mathbf{X} original points, blue circles - new points \mathbf{Y}_0 . (c) The original \mathbf{X} and the set \mathbf{Y} . \mathbf{Y} is the set of generated points after applying the MGC diffusion operator $\hat{\mathbf{P}}$ (steps 6-7 of Alg. 1). (d) The final set again colored by the degree value $\hat{d}(i)$ at each point.

ate the embedding $\mathbf{X}_{\text{phate}} = \{\bar{\mathbf{x}}_1, \bar{\mathbf{x}}_2, \dots, \bar{\mathbf{x}}_{1029}\}$, $\bar{\mathbf{x}}_i \in \mathbb{R}^2$ Moon et al. (2017). Using gene module expression profiles (see supplement) as confirmation, PHATE captured cellular development trajectories (figure 7(b)) similar to the supervised approach in Velten *et al.*

SUGAR was performed in this experiment on $\mathbf{X} = \{\mathbf{x}_1, \mathbf{x}_2, \dots, \mathbf{x}_{1029}\}$, $\mathbf{x}_i = [\tilde{\mathbf{x}}_i; \hat{\mathbf{x}}_i; \bar{\mathbf{x}}_i] \in \mathbb{R}^{12563}$, the concatenation of both experimental data types and the PHATE embedding. However, to generate points directly in sparse areas of the PHATE plot, sparsity was estimated in the PHATE dimensions (figure 7(a)). SUGAR yielded 1919 data points $\mathbf{Y} = \{\mathbf{y}_1, \mathbf{y}_2, \dots, \mathbf{y}_{1919}\}$, $\mathbf{y}_i \in \mathbb{R}^{12563}$ (figure 7(b)). Generating PHATE dimensions alongside the data allowed us to avoid repeating costly computational steps of PHATE such as running multi-dimensional scaling on the 1919 SUGAR points. A similar approach could be applied to any visualization technique or linked data set.

The total post-SUGAR size of the data is thus 2948, nearly triple the initial starting size. Despite this increase, geometry is maintained and faithful to biology. Rare transition populations spanning biological time between mature cells and the stem cell reservoir are enriched by SUGAR, augmenting phase transitions that were once completely sparse. Two examples of this restoration are present in this data. First, the granulocyte (neutrophils (N) and Eosinophil/Basophil/Mast Cells (EBM); Murphy & Weaver 2016) transition (top right branch of figure 7(a) labeled in 7(b)) is discontinuous between the dense neutrophil/stem-cell body and the dense EBM island. This is likely due to the abundance of neutrophils in the bloodstream, which may range between 40-70% of white blood cells in healthy individuals Murphy &

Weaver (2016). SUGAR repaired this discontinuity, illustrated by the EBM gene profile shown by the color in figure 7(c) (see supplement for gene profile information). Second, the original dataset contains a large gap between a dense plane of B-primed cells and a sparse island of more mature B cells (rightmost branch in figure 7(a), labeled in 7(b)). Notably, SUGAR recovered this trajectory, evidenced by transitional up-regulation of the B cell maturation marker *CD19* (figure 7(d)). These examples illustrate the ability of SUGAR to recover rare or difficult to capture populations while maintaining data geometry.

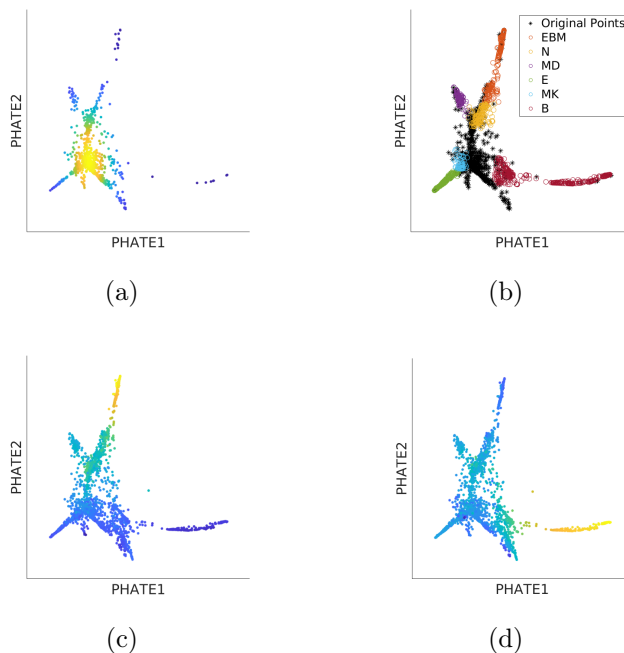


Figure 7: SUGAR recovers branching trajectories in hematopoiesis. (a) PHATE plot of the original Velten et al. (2017) data colored by the degree $\hat{d}(i)$. (b) PHATE plot of Velten et al. (2017) (black asterisks) data with SUGAR generated points \mathbf{Y} (circles) colored by genetic module profile (see supplement for gene module details). EBM: Eosinophil/Basophil/Mast Cells; N: Neutrophils; MD: Monocytes/Dendritic Cells; E: Erythroid; MK: Megakaryocyte; B: B cell. (c) EBM Module Expression. (d) *CD19* count after SUGAR. *CD19* is found in maturing B cells Murphy & Weaver (2016)

Finally, SUGAR was able to recover canonical gene-gene relationships not observed in the original data. We examined the relationship between two priming markers, *CASP1*, *HOXA3*, and the maturation marker *CD19*. Velten et al. (2017) confirms a positive relationship between *CASP1* and B-cell lineage commitment using a supervised method that accounts for gene ontology and co-expression. However, gaps in the original data obscures the relationship between *CASP1* and *CD19* as measured by correlation ($R = 0.364$) and mutual information ($MI = 1.04$) (figure 8(a)). SUGAR restored this relationship, increasing correlation ($R = 0.777$) and mutual information ($MI = 2.49$). Similarly, we attempted to confirm the negative relationship between *HOXA3*, which in the *HOXA3/HOXB6* module is associated with immature stem cells, and *CD19*. In the original data, sparsity obscured statis-

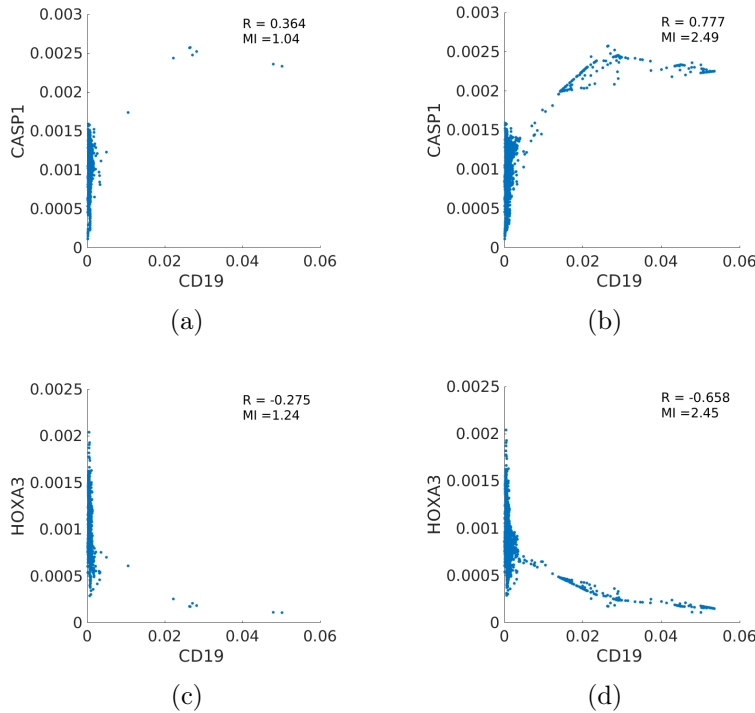


Figure 8: SUGAR restores canonical gene-gene relationships in B cell development. (a) Relationship between *Cok the whole ASP1* and *CD19* before SUGAR. The *CASP1/IRF1* module is a marker of B cell lineage commitment Velten et al. (2017). *CD19* is a marker of B-Cell maturity. (b) Relationship between *CASP1* and *CD19* after SUGAR. (c) Relationship between *HOXA3* and *CD19* before SUGAR. The *HOXA3/HOXB6* module marks non-committed stem cells Velten et al. (2017) (d) Relationship between *HOXA3* and *CD19* after SUGAR.

tical measures of this relationship ($R = -0.275$, $MI = 1.24$) (figure 8(c)); SUGAR yielded roughly two-fold improvement of these measures ($R = -0.658$, $MI = 2.45$; figure 8(d)).

In this experiment, we have demonstrated the ability of SUGAR to generate new points in multiple data types alongside manifold visualization dimensions. We have demonstrated the biological relevance of SUGAR. First, SUGAR tripled the dataset size without loss of geometry. In exploratory analysis, this facilitated cell type analysis and identification in regions that were once questionable due to sparsity. Second, SUGAR filled in branch discontinuities that were otherwise sparse in the original data. Restoring these regions increased the breath of the data set by incorporating previously rare transitional populations and under-sampled mature cells. Recovery of these populations strengthened the signal of canonical biological relationships in B cell development.

6 Conclusion

We proposed SUGAR a new type of generative model for data, based on learning geometry rather than the density of the data. This enables us to compensate for sparsity and heavily biased sampling in many data types of interest, especially

biomedical data. We assume that the training data lies on a low-dimensional manifold. The manifold assumption is usually valid as many datasets are globally high-dimensional but locally generated by a small number of factors. We use a diffusion kernel to capture the manifold structure. Then, we generate new points along the incomplete manifold by randomly generating points at sparse areas. Finally, we use a weighted transition kernel to pull the new points towards the structure of the manifold. The method demonstrated promising results on artificial points, Mnist images, a 3-D representation of a bunny and high dimensional biological measurement. In the future, we plan to use SUGAR to study extremely biased biological datasets and to improve classification performance on imbalanced training sets.

References

- Bermanis, Amit, Wolf, Guy, and Averbuch, Amir. Diffusion-based kernel methods on euclidean metric measure spaces. *Applied and Computational Harmonic Analysis*, 41(1):190–213, 2016.
- Bernardo, JM, Bayarri, MJ, Berger, JO, Dawid, AP, Heckerman, D, Smith, AFM, West, M, et al. The variational bayesian em algorithm for incomplete data: with application to scoring graphical model structures. *Bayesian statistics*, 7:453–464, 2003.
- Chan, Philip K and Stolfo, Salvatore J. Toward scalable learning with non-uniform class and cost distributions: A case study in credit card fraud detection. In *KDD*, volume 1998, pp. 164–168, 1998.
- Coifman, Ronald R. and Lafon, StÃlphane. Diffusion maps. *Applied and Computational Harmonic Analysis*, 21(1):5 – 30, 2006.
- He, Haibo and Garcia, Edwardo A. Learning from imbalanced data. *IEEE Transactions on knowledge and data engineering*, 21(9):1263–1284, 2009.
- Hensman, Paulina and Masko, David. The impact of imbalanced training data for convolutional neural networks. *Degree Project in Computer Science, KTH Royal Institute of Technology*, 2015.
- Keller, Yosi, Coifman, Ronald R, Lafon, StÃlphane, and Zucker, Steven W. Audio-visual group recognition using diffusion maps. *IEEE Transactions on Signal Processing*, 58(1):403–413, 2010.
- Kingma, Diederik P and Welling, Max. Auto-encoding variational bayes. *arXiv preprint arXiv:1312.6114*, 2013.
- Lindenbaum, Ofir, Bregman, Yuri, Rabin, Neta, and Averbuch, Amir. Multi-view kernels for low-dimensional modeling of seismic events. *arXiv preprint arXiv:1706.01750*, 2017a.
- Lindenbaum, Ofir, Salhov, Moshe, Yeredor, Arie, and Averbuch, Amir. Kernel scaling for manifold learning and classification. *arXiv preprint arXiv:1707.01093*, 2017b.

- López, Victoria, Fernández, Alberto, García, Salvador, Palade, Vasile, and Herrera, Francisco. An insight into classification with imbalanced data: Empirical results and current trends on using data intrinsic characteristics. *Information Sciences*, 250:113–141, 2013.
- Moon, Kevin R, van Dijk, David, Wang, Zheng, Burkhardt, Daniel, Chen, William, van den Elzen, Antonia, Hirn, Matthew J, Coifman, Ronald R, Ivanova, Natalia B, Wolf, Guy, et al. Visualizing transitions and structure for high dimensional data exploration. *bioRxiv*, pp. 120378, 2017.
- Murphy, Kenneth and Weaver, Casey. *Janeway’s immunobiology*. Garland Science, 2016.
- Rasmussen, Carl Edward. The infinite gaussian mixture model. In *Advances in neural information processing systems*, pp. 554–560, 2000.
- Scott, David W. Kernel density estimators. *Multivariate Density Estimation: Theory, Practice, and Visualization*, pp. 125–193, 2008.
- Singer, Amit, Erban, Radek, Kevrekidis, Ioannis G, and Coifman, Ronald R. Detecting intrinsic slow variables in stochastic dynamical systems by anisotropic diffusion maps. *Proceedings of the National Academy of Sciences*, 106(38):16090–16095, 2009.
- Van Den Bosch, Antal, Weijters, A, Van Den Herik, H Jaap, and Daelemans, Walter. When small disjuncts abound, try lazy learning: A case study. In *Proceedings of the Seventh Belgian-Dutch Conference on Machine Learning*, pp. 109–118, 1997.
- Velten, Lars, Haas, Simon F, Raffel, Simon, Blaszkiewicz, Sandra, Islam, Saiful, Hennig, Bianca P, Hirche, Christoph, Lutz, Christoph, Buss, Eike C, Nowak, Daniel, et al. Human haematopoietic stem cell lineage commitment is a continuous process. *Nat. Cell Biol*, 19:271–281, 2017.
- Weiss, Gary M. Mining with rarity: a unifying framework. *ACM Sigkdd Explorations Newsletter*, 6(1):7–19, 2004.
- Zelnik-Manor, Lihi and Perona, Pietro. Self-tuning spectral clustering. In *Advances in neural information processing systems*, pp. 1601–1608, 2005.